

Quark-hadron duality constraints on γZ box corrections to parity-violating elastic scattering

N. L. Hall^a, P. G. Blunden^a, W. Melnitchouk^b, A. W. Thomas^c, R. D. Young^c

^a*Department of Physics and Astronomy, University of Manitoba, Winnipeg, MB, Canada R3T 2N2*

^b*Jefferson Lab, 12000 Jefferson Avenue, Newport News, Virginia 23606, USA*

^c*ARC Centre of Excellence for Particle Physics at the Terascale and CSSM, Department of Physics, University of Adelaide, Adelaide SA 5005, Australia*

Abstract

We examine the interference γZ box corrections to parity-violating elastic electron–proton scattering in the light of the recent observation of quark-hadron duality in parity-violating deep-inelastic scattering from the deuteron at low Q^2 . Using the similarity of electromagnetic and γZ structure function moments and those extracted from leading twist parton distributions down to $Q^2 \approx 1 \text{ GeV}^2$, we find that duality constrains the γZ box correction to $\Re \square_{\gamma Z}^V = (5.4 \pm 0.4) \times 10^{-3}$ at the kinematics of the Q_{weak} experiment. Within the same model we also provide estimates of the γZ corrections for future experiments, such as MOLLER at Jefferson Lab and MESA at Mainz.

Keywords: Parity violation, proton weak charge, quark-hadron duality

1. Introduction

Parity-violating precision measurements have for many years provided crucial low-energy tests of the Standard Model. Early efforts such as the E122 experiment at SLAC [1, 2] firmly established the $SU(2) \times U(1)$ model as the theory of the unified electroweak interactions. Modern-day experiments use parity violation to probe physics beyond the Standard Model. One of the most recent parity-violating measurements is the Q_{weak} experiment at Jefferson Lab [3], which aims to measure the proton’s weak charge to 4% accuracy. With an initial analysis of a subset of the data already reported [4], the analysis of the full data set is expected in the near future.

For the precision requirements of the Q_{weak} experiment, the weak charge of the proton, defined at tree level as $Q_W^p = 1 - 4 \sin^2 \theta_W$, must also include radiative corrections. Including corrections at the 1-loop level, the weak charge can be written as [5]

$$Q_W^p = (1 + \Delta\rho + \Delta_e) \left(1 - 4 \sin^2 \theta_W(0) + \Delta_e' \right) + \square_{WW} + \square_{ZZ} + \square_{\gamma Z}(0), \quad (1)$$

where $\sin^2 \theta_W(0)$ is the weak mixing angle at zero momentum transfer, and the electroweak vertex and neutral current correction terms $\Delta\rho$, Δ_e and Δ_e' have been calculated to the necessary levels of precision [5]. The weak box corrections \square_{WW} and \square_{ZZ} are dominated by short-distance effects and can also be computed perturbatively to the required accuracy.

On the other hand, the final term in Eq. (1), the γZ box contribution, depends on both short- and long-distance physics and therefore requires nonperturbative input. Considerable attention has been given to the analysis of this term, for both the vector electron–axial vector hadron coupling to the Z , $\square_{\gamma Z}^A$ (which is relevant for atomic parity violation experiments) [6, 7, 8, 9] and the axial electron–vector hadron coupling, $\square_{\gamma Z}^V$ (which because of its strong energy dependence makes important contributions to the Q_{weak} experiment) [10, 11, 12, 13, 14]. The most accurate technique to evaluate the latter is a dispersion relation. While constraints from parton distribution functions (PDFs) and recent parity-violating deep-inelastic scattering (PVDIS) data [15, 16] provide a systematic way of reducing the errors on this correction [14], some uncertainty remains about the model dependence of the low- Q^2 input.

The E08-011 electron–deuteron PVDIS experiment at Jefferson Lab not only allowed an accurate determination of the C_{2q} electron–quark effective weak couplings [16], but also presented the first direct evidence

for quark-hadron duality in γZ interference structure functions, which was verified at the (10–15)% level for Q^2 down to $\approx 1 \text{ GeV}^2$ [15]. In general, quark-hadron duality refers to the similarity of low-energy hadronic cross sections, averaged over resonances, with asymptotic cross sections, calculated at the parton level and extrapolated to the resonance region. It is manifested in many different hadronic observables [17] and was first observed in deep-inelastic scattering by Bloom and Gilman [18, 19]. Subsequent studies have quantified the validity of duality for various spin-averaged and spin-dependent electromagnetic structure functions, as well as in neutrino scattering and for different targets [20, 21, 22, 23, 24, 25, 26, 27], establishing the phenomenon as a general feature of the strong interaction.

Here we discuss the extent to which quark-hadron duality in γZ structure functions can provide additional constraints on the $\square_{\gamma Z}^V$ corrections, in particular, the contributions from low Q^2 and low hadronic final state masses W . In Sec. 2 we discuss the validity of quark-hadron duality for moments of the electromagnetic and γZ structure functions. From the observed description of the phenomenological structure function moments in terms of leading twist (LT) PDFs down to $Q^2 \approx 1 \text{ GeV}^2$, we explore the consequences for the energy dependence of the $\square_{\gamma Z}^V$ correction in Sec. 3, and especially the limits on its overall uncertainty. Finally, in Sec. 4 we summarize our findings and discuss their implications for the analysis of the Q_{weak} experiment as well as possible future parity-violating experiments.

2. Duality in electromagnetic and γZ structure functions

Historically, the observation of duality in inclusive electron scattering [18, 19] predates the development of QCD and was initially formulated in the language of finite-energy sum rules. Within QCD, duality was reinterpreted within the operator product expansion through moments of structure functions [28], with duality violations associated with matrix elements of higher twist (HT) operators describing nonperturbative, multi-parton physics.

2.1. Moments of structure functions

The extent to which inclusive lepton–nucleon cross sections can be described by incoherent scattering from individual partons through LT PDFs can be quantified by studying the Q^2 dependence of the structure function moments. At low Q^2 , corrections to the LT results arise not only from multi-parton processes, but also from kinematical target mass corrections (TMCs), which, although $1/Q^2$ suppressed, arise from LT operators. To isolate the genuine duality-violating HT effects, one can consider Nachtmann moments of structure functions [29], which are constructed to explicitly remove the effects of higher spin operators and the resulting TMCs. Specifically, for the F_1 and F_2 structure functions one has [30]

$$\mu_1^{(n)}(Q^2) = \int_0^1 dx \frac{\xi^{n+1}}{x^3} \left[x F_1(x, Q^2) + \frac{1}{2} \rho^2 \eta_n F_2(x, Q^2) \right], \quad (2)$$

$$\mu_2^{(n)}(Q^2) = \int_0^1 dx \frac{\xi^{n+1}}{x^3} \rho^2 (1 + 3\eta_n) F_2(x, Q^2), \quad (3)$$

where

$$\xi = \frac{2x}{1 + \rho} \quad (4)$$

is the Nachtmann scaling variable [30, 31], with $x = Q^2/(W^2 - M^2 + Q^2)$ the Bjorken scaling variable, $\rho^2 = 1 + 4M^2x^2/Q^2$, and M the nucleon mass. The variable η_n is given by

$$\eta_n = \frac{\rho - 1}{\rho^2} \left[\frac{n + 1 - (\rho + 1)(n + 2)}{(n + 2)(n + 3)} \right], \quad (5)$$

which vanishes in the $Q^2 \rightarrow \infty$ limit. In that limit the moments $\mu_i^{(n)}$ approach the standard Cornwall-Norton moments [32],

$$\mu_i^{(n)}(Q^2) \longrightarrow M_i^{(n)}(Q^2) = \int_0^1 dx x^{n-i} F_i(x, Q^2), \quad i = 1, 2. \quad (6)$$

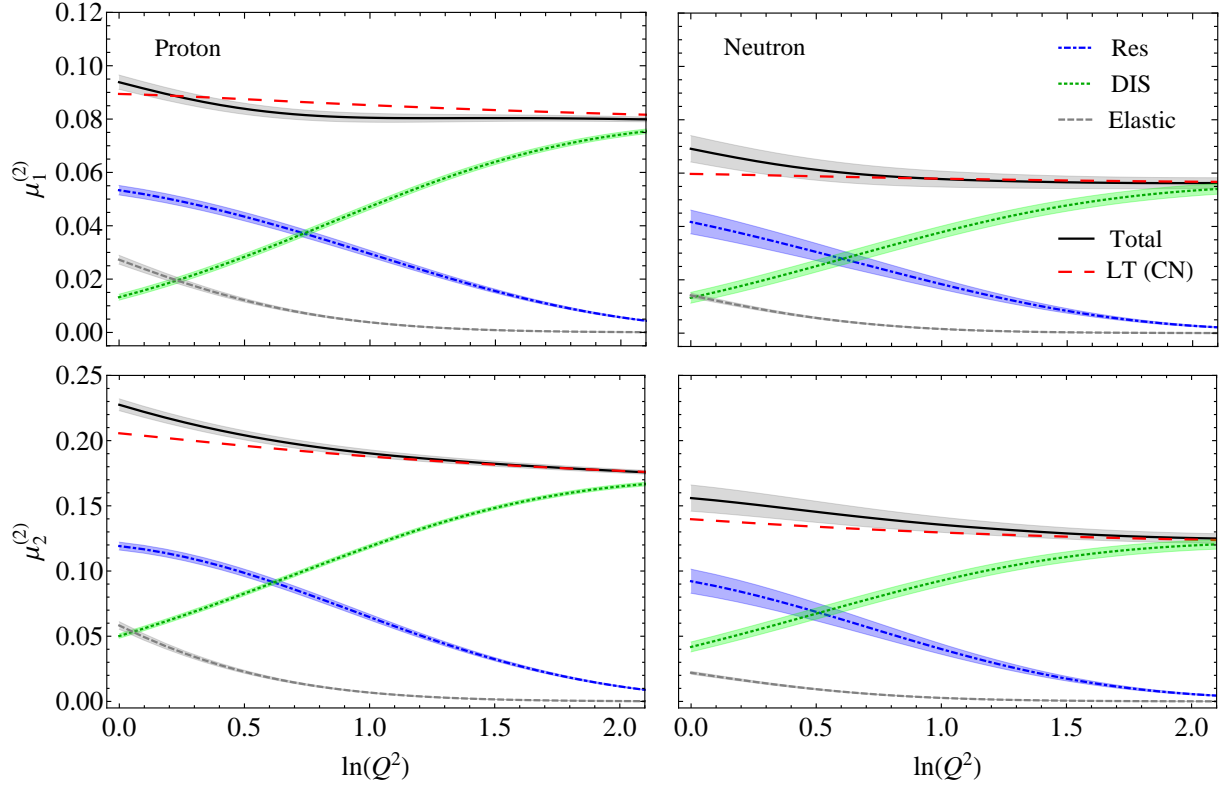


Figure 1: The proton (left panels) and neutron (right panels) electromagnetic $F_1^{\gamma\gamma}$ (top) and $F_2^{\gamma\gamma}$ (bottom) structure function moments. The total Nachtmann moments (black solid lines) include contributions from the resonance ($W^2 \leq 6 \text{ GeV}^2$, blue dot-dashed lines) and DIS ($W^2 > 6 \text{ GeV}^2$, green dotted lines) regions, as well as the elastic contributions (gray dashed lines), and are compared with the Cornwall-Norton moment of the LT structure functions (red long-dashed lines).

At finite Q^2 , while the $\mu_2^{(n)}$ moment depends only on the F_2 structure function, the $\mu_1^{(n)}$ moment has contributions from both the F_1 and F_2 structure functions. Because the latter contribution is proportional to η_n , it vanishes at large Q^2 , so that the $\mu_1^{(n)}$ moment is generally dominated by the F_1 structure function at large Q^2 . Note also that the notation for $\mu_1^{(n)}$ and $\mu_2^{(n)}$ in Eqs. (2) and (3) differs from that used in Refs. [29, 30].

2.2. Electromagnetic structure functions

Duality in the nucleon's unpolarized electromagnetic structure functions has been studied most extensively for the F_2 structure function [20, 21, 33], and to a lesser extent for the F_1 (or longitudinal F_L) structure function [17, 34]. The latter is generally more difficult to access experimentally, as it requires precise longitudinal-transverse separated cross section measurements, or equivalently the σ_L/σ_T cross section ratio.

The $n = 2$ Nachtmann moments of the proton and neutron $F_1^{\gamma\gamma}$ and $F_2^{\gamma\gamma}$ structure functions are shown in Fig. 1 over the range $1 \leq Q^2 \leq 8 \text{ GeV}^2$. For the low- W^2 contributions, $W^2 \leq 6 \text{ GeV}^2$, we use the resonance-based fit to the electromagnetic structure function data from Christy and Bosted [35]. For the DIS region at higher W^2 values, $W^2 > 6 \text{ GeV}^2$, this is supplemented by the ABM global QCD fit [36] to high-energy data, which includes LT, TMC and HT contributions. Since LT evolution is logarithmic in Q^2 , at large Q^2 the moments are predicted to become flat in $\ln Q^2$. While the individual resonance and DIS region contributions, as well as the elastic ($W = M$) component, are strongly Q^2 dependent in the region of low Q^2 shown in Fig. 1, remarkably their sum exhibits very mild Q^2 dependence down to $Q^2 \approx 1 \text{ GeV}^2$. This is the classic manifestation of duality observed by Bloom and Gilman [18, 19], in which the total empirical moments

resemble the LT contributions down to surprisingly low momentum scales. Note that since the Nachtmann moments are constructed to remove higher spin operators that are responsible for TMCs, in the absence of HTs one would expect that the Nachtmann moments of the total structure functions would resemble the Cornwall-Norton moments of the LT functions, $\mu_i^{(n)}(\text{LT} + \text{TMC}) = M_i^{(n)}(\text{LT})$ [37].

This expectation is clearly borne out for the $\mu_1^{(2)}$ and $\mu_2^{(2)}$ moments in Fig. 1. At $Q^2 = 1 \text{ GeV}^2$ the LT proton and neutron $F_1^{\gamma\gamma}$ moments are $\approx 5\%$ and $\approx 14\%$ smaller than the full moments, respectively, while for $F_2^{\gamma\gamma}$ the LT moments are $\approx 10\%$ smaller than the full results for both the proton and neutron. At large Q^2 the duality violations are generally $\lesssim 5\%$ for all moments. Following Ref. [35], we assign a 5% error on the proton $F_1^{\gamma\gamma}$ and $F_2^{\gamma\gamma}$ structure functions, and a larger, 10% error on the neutron structure function [38], reflecting the additional nuclear model dependence in extracting the latter from deuterium data [39]. For the elastic contribution a 5% uncertainty is assumed for the total elastic structure functions from Ref. [40].

2.3. γZ structure functions

Experimental information on the interference γZ structure functions is for the most part nonexistent, with the exception of some measurements of $F_2^{\gamma Z}$ and $xF_3^{\gamma Z}$ at HERA at very high Q^2 [41], where the γZ contribution becomes comparable to the purely electromagnetic component of the neutral current. In particular, there are no direct measurements of $F_1^{\gamma Z}$ and $F_2^{\gamma Z}$ in the $Q^2 \sim \text{few GeV}^2$ range that is relevant for the evaluation of the γZ box correction to Q_W^p [14].

Several previous phenomenological analyses [42, 43, 44] of high-energy scattering data have found no indication of strong isospin dependence of HT corrections. To the extent that duality violations are determined by the size of HT contributions, one may therefore expect qualitatively similar manifestations of quark-hadron duality for γZ structure functions as for the electromagnetic analogs. The degree to which duality holds in the $F_1^{\gamma Z}$ and $F_2^{\gamma Z}$ structure function moments can be quantified by considering their Nachtmann moments, as for the electromagnetic moments in Fig. 1. In Refs. [14, 45] the $F_1^{\gamma Z}$ and $F_2^{\gamma Z}$ structure functions were computed from the phenomenological Adelaide-Jefferson Lab-Manitoba (AJM) parametrization. This is based on the electromagnetic structure functions described in Sec. 2.2, but appropriately rotated to the γZ case according to the specific W^2 and Q^2 region considered, with the rotation parameters constrained by phenomenological PDFs [14] and recent PVDIS data [15, 16].

The resulting Nachtmann moments of the $F_1^{\gamma Z}$ and $F_2^{\gamma Z}$ structure functions are shown in Fig. 2 for the proton and neutron, over the same kinematic range as the electromagnetic moments in Fig. 1. The uncertainties on the proton γZ structure functions are taken to be the same as those used in the $\Box_{\gamma Z}^V$ calculation in Ref. [14], while the neutron structure functions are assigned a 15% error to take into account the additional uncertainty when extracting free neutron information from deuteron cross sections. A 5% uncertainty is assumed for both the proton and neutron elastic γZ structure functions.

As for the electromagnetic structure function moments, the results for the interference $\mu_1^{(2)\gamma Z}$ and $\mu_2^{(2)\gamma Z}$ moments show good agreement between the full moments and the LT contributions. At $Q^2 = 1 \text{ GeV}^2$, for example, the LT proton and neutron $F_1^{\gamma Z}$ moments are $\approx 23\%$ and $\approx 20\%$ smaller than the corresponding full moments. For the $F_2^{\gamma Z}$ moments duality holds to even better accuracy, with differences between the full and LT moments $\approx 11\%$ for the proton and $\approx 6\%$ for the neutron. Beyond $Q^2 = 2 \text{ GeV}^2$, duality in the moments holds to $\lesssim 7\%$ for all structure functions.

That the level of agreement shown in Fig. 2 between the $F_1^{\gamma Z}$ and $F_2^{\gamma Z}$ structure function moments calculated in the AJM model and the LT values is consistent with the accuracy of duality for the electromagnetic case provides additional evidence for the reliability of the AJM model. This comes on top of the recent empirical evidence of duality from the deuteron PVDIS asymmetry measurement at Jefferson Lab for $Q^2 \approx 0.8 - 1.5 \text{ GeV}^2$ [15]. Together these support the idea that estimate of the uncertainty in the AJM model is rather conservative, and can serve to provide an important additional constraint on the $\Box_{\gamma Z}^V$ correction to Q_W^p , as we discuss next.

3. Implications for γZ box corrections to Q_W^p

The real part of the γZ box correction which enters in Eq. (1) can be determined from an unsubtracted dispersion relation [10, 11, 12, 13, 14],

$$\Re \Box_{\gamma Z}^V(E) = \frac{2E}{\pi} \mathcal{P} \int_0^\infty dE' \frac{1}{E'^2 - E^2} \Im m \Box_{\gamma Z}^V(E'), \quad (7)$$

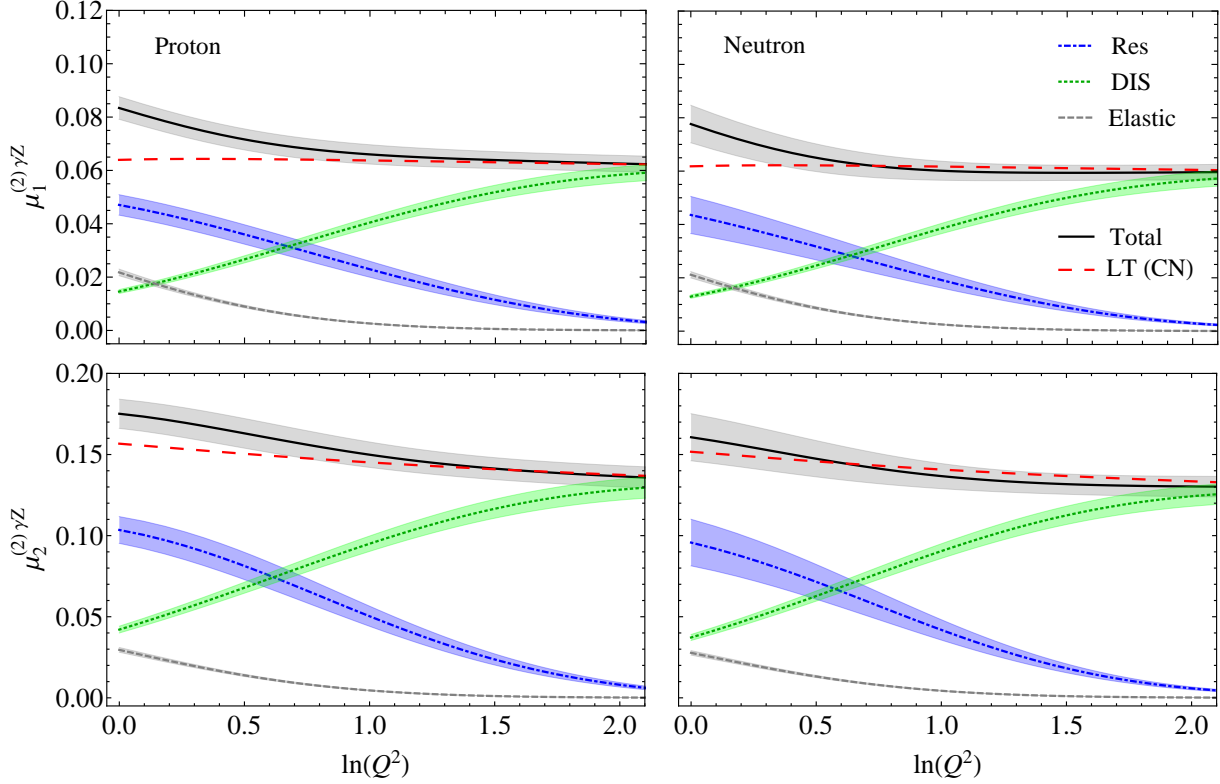


Figure 2: As in Fig. 1, but for the interference γZ structure function moments $\mu_1^{(2)\gamma Z}$ (top panels) and $\mu_2^{(2)\gamma Z}$ (bottom panels).

where \mathcal{P} is the Cauchy principal value integral, and the imaginary part of $\Box_{\gamma Z}^V$ is given in terms of the $F_1^{\gamma Z}$ and $F_2^{\gamma Z}$ interference structure functions,

$$\Im m \Box_{\gamma Z}^V(E) = \frac{1}{(s - M^2)^2} \int_{W_\pi^2}^s dW^2 \int_0^{Q_{\max}^2} dQ^2 \frac{\alpha(Q^2)}{1 + Q^2/M_Z^2} \left[F_1^{\gamma Z} + \frac{s(Q_{\max}^2 - Q^2)}{Q^2(W^2 - M^2 + Q^2)} F_2^{\gamma Z} \right]. \quad (8)$$

Here α is the running electromagnetic coupling evaluated at the scale Q^2 , and M_Z is the Z boson mass. The W^2 range covered in the integral lies between the inelastic threshold, $W_\pi^2 = (M + m_\pi)^2$ and the total electron–proton center of mass energy squared, $s = M^2 + 2ME$, while the Q^2 integration range is from 0 up to $Q_{\max}^2 = 2ME(1 - W^2/s)$. (The small mass of the electron is neglected throughout.) Note that while the dispersion relation (7) is valid only for forward scattering, because the Q_{weak} experiment is performed at a small scattering angle $\approx 6^\circ$, in practice it provides a very good approximation.

From the structure of the dispersion integral (7), at low energies $E \sim 1$ GeV the bulk of the contribution to $\Re \Box_{\gamma Z}^V$ comes from the region of relatively low Q^2 and W^2 [13, 14]. While at high Q^2 and W^2 the $F_1^{\gamma Z}$ and $F_2^{\gamma Z}$ structure functions can be reliably determined in terms of universal PDFs, in the region most relevant for Q_{weak} the γZ structure functions have not been directly measured and must be modeled or inferred indirectly.

In previous analyses using the AJM model of the γZ structure functions [14, 45], the integral over Q^2 and W^2 in Eq. (8) has been split into three distinct regions, characterized by rather different physical mechanisms underlying the scattering process. In each region the most accurate parametrizations or models available for the appropriate kinematics have been used. At low Q^2 and W^2 , for example, resonance-based parametrizations of the electromagnetic and γZ structure functions were employed, as in the moment calculations in Figs. 1 and 2, while Regge theory-based models were used to describe the low Q^2 and high W^2 region. In

the DIS region at high Q^2 and high W^2 , the ABM global QCD fit [36] was utilized, which includes LT as well as subleading $1/Q^2$ TMC and HT contributions.

In the present analysis, we slightly modify the boundaries between the regions to reflect the application of duality in using a LT description to lower Q^2 values than in Ref. [14, 45]. In particular, we define “Region I” (low Q^2 , low W^2) to encompass $0 \leq Q^2 \leq 10 \text{ GeV}^2$ for $W_\pi^2 \leq W^2 \leq 4 \text{ GeV}^2$, and $Q^2 \leq 1 \text{ GeV}^2$ for $4 < W^2 \leq 9 \text{ GeV}^2$, using the $\gamma\gamma \rightarrow \gamma Z$ rotated Christy-Bosted structure function parametrization [35]. For “Region II” (low Q^2 , high W^2) the vector meson dominance + Regge model of Alwall and Ingelman [46] is used over the range $0 \leq Q^2 \leq 1 \text{ GeV}^2$ and $W^2 > 9 \text{ GeV}^2$. Finally, for “Region III” (high Q^2 , high W^2) the QCD-based global fit from Alekhin *et al.* [36] is used for $Q^2 > 1 \text{ GeV}^2$ and $W^2 > 4 \text{ GeV}^2$. The main distinction between the present treatment and that in Refs. [14, 45] is the extension of the boundary with Region III from $Q^2 = 2.5 \text{ GeV}^2$ down to $Q^2 = 1 \text{ GeV}^2$. Consistent with the duality constraint assumed in this analysis, in Region III we use the LT structure functions rather than the total functions which include the small subleading contributions [36]. This approach is supported by the good agreement between the LT and total moments observed in Figs. 1 and 2, and removes the additional uncertainty about the $\gamma\gamma \rightarrow \gamma Z$ rotation of the non-LT contributions to the structure functions, which in this case are obtained by the simple replacement of quark charges $e_q \rightarrow g_V^q$. For $x = 1$, the elastic contributions to the structure functions are computed using the form factor parametrizations from Ref. [40].

Within the AJM γZ structure function parametrization, the most uncertain elements are the $\kappa_C^{T,L}$ continuum parameters used to relate the high-mass, non-resonant continuum part of the γZ transverse and longitudinal cross sections to the $\gamma\gamma$ cross sections in the generalized vector meson dominance model [46, 47]. In the present analysis, we fit the $\kappa_C^{T,L}$ parameters by matching the γZ to $\gamma\gamma$ cross section ratios with the LT structure function ratios at the scale $Q^2 = 1 \text{ GeV}^2$,

$$\frac{\sigma_T^{\gamma Z}(\kappa_C^T)}{\sigma_T^{\gamma\gamma}} = \frac{F_1^{\gamma Z}}{F_1^{\gamma\gamma}} \Big|_{\text{LT}}, \quad \frac{\sigma_L^{\gamma Z}(\kappa_C^L)}{\sigma_L^{\gamma\gamma}} = \frac{F_L^{\gamma Z}}{F_L^{\gamma\gamma}} \Big|_{\text{LT}}, \quad (9)$$

where the longitudinal structure function F_L is related to the F_1 and F_2 structure functions by $F_L = \rho^2 F_2 - 2x F_1$ [14]. The resulting fit values,

$$\kappa_C^T = 0.36 \pm 0.15, \quad \kappa_C^L = 1.5 \pm 3.1, \quad (10)$$

are obtained by averaging over the $\kappa_C^{T,L}$ parameter determined from 10 fits with the ratios in Eq. (9) matched at between $W^2 = 4 \text{ GeV}^2$ and 13 GeV^2 . These values are then used to compute the γZ structure functions in the dispersion integral for $1 \leq Q^2 \leq 10 \text{ GeV}^2$ and $W_\pi^2 \leq W^2 \leq 4 \text{ GeV}^2$. To allow for stronger violations of duality at lower Q^2 , the uncertainties on $\kappa_C^{T,L}$ are inflated to 100% for the region $0 \leq Q^2 < 1 \text{ GeV}^2$ for all W^2 .

Using the AJM γZ structure functions obtained from the new fitted $\kappa_C^{T,L}$ values, the $\Re \square_{\gamma Z}^V$ correction is displayed in Fig. 3 as a function of beam energy, with a breakdown of the individual contributions from different regions given in Table 1. At the incident beam energy $E = 1.165 \text{ GeV}$ of the Q_{weak} experiment, the total correction is found to be

$$\Re \square_{\gamma Z}^V = (5.4 \pm 0.4) \times 10^{-3}. \quad (11)$$

Table 1: Contributions to $\Re \square_{\gamma Z}^V$ from Regions I, II and III, and the total, at the kinematics of the Q_{weak} , MOLLER, and MESA experiments.

Region	$\Re \square_{\gamma Z}^V (\times 10^{-3})$		
	Q_{weak} ($E = 1.165 \text{ GeV}$)	MOLLER ($E = 11 \text{ GeV}$)	MESA ($E = 0.18 \text{ GeV}$)
I	4.3 ± 0.4	2.5 ± 0.3	1.0 ± 0.1
II	0.4 ± 0.05	3.2 ± 0.5	0.06 ± 0.01
III	0.7 ± 0.04	5.5 ± 0.3	0.1 ± 0.01
Total	5.4 ± 0.4	11.2 ± 0.6	1.2 ± 0.1

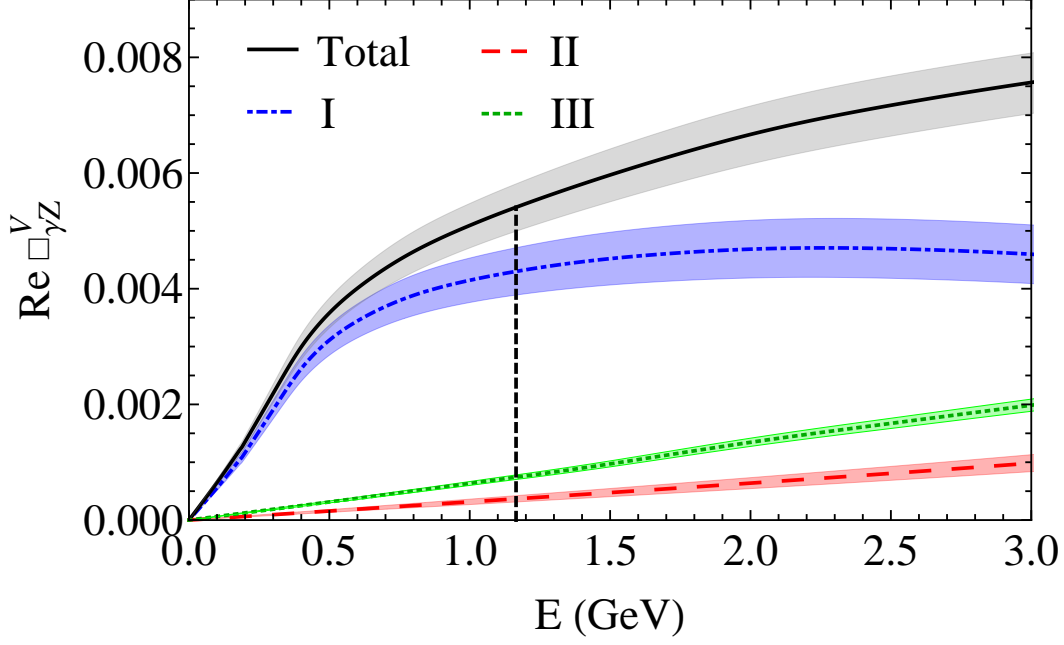


Figure 3: Energy dependence of the γZ box correction to Q_W^p . The contributions from various regions in W^2 and Q^2 (Regions I, II and III) are shown separately, as is the total (solid curve). The dashed vertical line refers to the beam energy $E = 1.165$ GeV of the Jefferson Lab Q_{weak} experiment.

This is in good agreement with the value $\Re \square_{\gamma Z}^V = (5.57 \pm 0.36) \times 10^{-3}$ found in the previous analysis [14]. In particular, even though the values of the continuum rotation parameters in the earlier fit were somewhat different ($\kappa_C^T = 0.65 \pm 0.14$ and $\kappa_C^L = -1.3 \pm 1.7$ with matching to the total DIS structure functions at $Q^2 = 2.5$ GeV²), the central value of $\Re \square_{\gamma Z}^V$ remains relatively unaffected.

The overall relative uncertainty has increased marginally from 7.5% to 9%, despite the rather more conservative estimates of the structure function uncertainty for $Q^2 \lesssim 1$ GeV² through the inflated errors on $\kappa_C^{T,L}$. Note that the same 100% uncertainties are used in the transformation of the vector meson dominance model [46, 47] in Region II. For Region III, the LT $F_1^{\gamma Z}$ and $F_2^{\gamma Z}$ structure functions are assigned a 5% uncertainty for $Q^2 \geq 2.5$ GeV², which is increased linearly to 10% at $Q^2 = 1.0$ GeV².

In the end, the largest contribution to $\Re \square_{\gamma Z}^V$ is still from Region I ($\approx 80\%$ of the total), with its error dominating the total uncertainty. The contributions from Regions II and III are $\approx 7\%$ and $\approx 13\%$ of the total at the Q_{weak} energy, but become more important with increasing energy. Interestingly, the modified Q^2 boundary for Region III results in a somewhat smaller contribution from Region II (0.4×10^{-3} compared with 0.6×10^{-3}), while the Region III contribution has doubled (0.7×10^{-3} compared with 0.35×10^{-3}) compared with that in Ref. [14].

Since the electromagnetic structure functions are reasonably well approximated by the LT results even below the traditional resonance–DIS boundary of $W^2 = 4$ GeV², we also examine the effect of lowering the W^2 cut into the peripheral resonance region down to $W^2 = 3$ GeV². In this case the contribution from Region III increases to 0.9×10^{-3} , while that from Region I correspondingly decreases to 4.2×10^{-3} , or $\approx 76\%$ of the total.

At the higher $E = 11$ GeV energy of the planned MOLLER experiment at Jefferson Lab [48], the DIS region contributes about half of the total, $\Re \square_{\gamma Z}^V = (11.2 \pm 0.6) \times 10^{-3}$, with Regions I and II making up the other 50%. This again agrees well with the earlier determination $\Re \square_{\gamma Z}^V = (11.5 \pm 0.8) \times 10^{-3}$ from Ref. [45]. On the other hand, for the possible future MESA experiment in Mainz [49] at a lower energy, $E = 0.18$ GeV, the bulk of the contribution still comes from Region I, but is reduced by a factor of ~ 4 compared with the correction at the Q_{weak} energy.

4. Conclusion

Quark-hadron duality is one of the most remarkable phenomena ever observed in hadronic physics. While some aspects of global duality can be formulated in the language of QCD, such as the relation between the scale independence of structure function moments and the size of higher twists, the detailed workings of local duality, for specific regions of W^2 or x , are not well understood from first principles. Nevertheless, there are many marvellous practical applications to which duality can be put. For example, the high-energy behavior of hadronic cross sections can be used to predict averages of resonance properties; and, conversely, low- W^2 data, suitably averaged, can be utilized to constrain LT parton distributions in difficult to access kinematic regions.

The latter category appears the most promising approach at present, with several global PDF analyses [36, 44, 39] extending their coverage down to lower Q^2 ($Q^2 \gtrsim 1 \text{ GeV}^2$) and W^2 ($W^2 \gtrsim 3 \text{ GeV}^2$) values than in traditional LT analyses. This not only increases considerably the available data base for PDF fitting, it is also one of the few ways currently available to study PDFs at high $x \sim 1$. In this spirit we have explored the realization of quark-hadron duality in γZ interference structure functions within the AJM model, finding a similar level of duality exhibited by the $F_1^{\gamma Z}$ and $F_2^{\gamma Z}$ structure functions as for their electromagnetic counterparts.

The main implication of duality for the current analysis is the extension of the LT description of γZ structure functions to lower Q^2 , $Q^2 = 1 \text{ GeV}^2$, than in previous work [14]. This serves to reduce the size of the contribution from Region I, which has the largest uncertainty associated with the behavior of the γZ structure functions at low Q^2 and W^2 . To account for the possible model dependence of the $\gamma\gamma \rightarrow \gamma Z$ structure function rotation and the violation of duality at low Q^2 , we have assigned rather conservative errors on $F_1^{\gamma Z}$ and $F_2^{\gamma Z}$ in this region. This is reflected in the increased uncertainty on this contribution, which is somewhat offset by the larger contribution from Region III, which is constrained by PDFs.

The final result of $\Re \Box_{\gamma Z}^V = (5.4 \pm 0.4) \times 10^{-3}$, is consistent with our previous analysis [14], but with a slightly larger relative uncertainty. It also agrees with the central value from Ref. [13], although the error there is ≈ 5 times larger, which in view of our current analysis appears to be somewhat overestimated. Our findings suggest that with the constraints from existing PVDIS data and PDFs, and now with the further support from quark-hadron duality, the overall uncertainty in the estimate of the γZ box correction is well within the range needed for an unambiguous extraction of the weak charge from the Q_{weak} experiment.

Further reduction of the uncertainty on the γZ correction will come from new measurements of PVDIS asymmetries on the proton, particularly at the low Q^2 and W^2 values that are most relevant at the Q_{weak} energy. These will also be useful in constraining the γZ contribution at the much lower energy $E = 0.18 \text{ GeV}$ of the MESA experiment [49], where we find the correction to be ≈ 4 times smaller but even more dominated by Region I. In contrast, for the MOLLER experiment at the higher $E = 11 \text{ GeV}$ energy the dispersion integral is dominated by the DIS region, which although contributing to a larger overall $\Box_{\gamma Z}^V$ correction, is better determined in terms of PDFs. These new experiments hold the promise of allowing the most precise low-energy determination of the weak mixing angle to date, and providing a unique window on possible new physics beyond the Standard Model.

Acknowledgements

This work was supported by NSERC (Canada), the DOE Contract No. DE-AC05-06OR23177, under which Jefferson Science Associates, LLC operates Jefferson Lab, and the Australian Research Council through an Australian Laureate Fellowship (A.W.T.), a Future Fellowship (R.D.Y.) and through the ARC Centre of Excellence for Particle Physics at the Terascale.

References

- [1] C. Y. Prescott *et al.*, Phys. Lett. B **77** (1978) 347.
- [2] C. Y. Prescott *et al.*, Phys. Lett. B **84** (1979) 524.
- [3] D. S. Armstrong *et al.*, arXiv:1202.1255.

- [4] D. Androic *et al.*, Phys. Rev. Lett. **111** (2013) 141803.
- [5] J. Erler, A. Kurylov and M. J. Ramsey-Musolf, Phys. Rev. D **68** (2003) 016006.
- [6] W. J. Marciano and A. Sirlin, Phys. Rev. D **27** (1983) 552.
- [7] W. J. Marciano and A. Sirlin, Phys. Rev. D **29** (1984) 75.
- [8] P. G. Blunden, W. Melnitchouk and A. W. Thomas, Phys. Rev. Lett. **107** (2011) 081801.
- [9] P. G. Blunden, W. Melnitchouk and A. W. Thomas, Phys. Rev. Lett. **109** (2012) 262301.
- [10] M. Gorchtein and C. J. Horowitz, Phys. Rev. Lett. **102** (2009) 091806.
- [11] A. Sibirtsev, P. G. Blunden, W. Melnitchouk and A. W. Thomas, Phys. Rev. D **82** (2010) 013011.
- [12] B. C. Rislow and C. E. Carlson, Phys. Rev. D **83** (2011) 113007.
- [13] M. Gorchtein, C. J. Horowitz and M. J. Ramsey-Musolf, Phys. Rev. C **84** (2011) 015502.
- [14] N. L. Hall, P. G. Blunden, W. Melnitchouk, A. W. Thomas and R. D. Young, Phys. Rev. D **88** (2013) 013011.
- [15] D. Wang *et al.*, Phys. Rev. Lett. **111** (2013) 082501.
- [16] D. Wang *et al.*, Nature **506** (2014) 67.
- [17] W. Melnitchouk, R. Ent and C. E. Keppel, Phys. Rept. **406** (2005) 127.
- [18] E. D. Bloom and F. J. Gilman, Phys. Rev. Lett. **25** (1970) 1140.
- [19] E. D. Bloom and F. J. Gilman, Phys. Rev. D **4** (1971) 2901.
- [20] I. Niculescu *et al.*, Phys. Rev. Lett. **85** (2000) 1186.
- [21] I. Niculescu *et al.*, Phys. Rev. Lett. **85** (2000) 1182.
- [22] A. Airapetian *et al.*, Phys. Rev. Lett. **90** (2003) 092002.
- [23] J. Arrington, R. Ent, C. E. Keppel, J. Mammei and I. Niculescu, Phys. Rev. C **73** (2006) 035205.
- [24] F. R. Wesselmann *et al.*, Phys. Rev. Lett. **98** (2007) 132003.
- [25] A. Psaker, W. Melnitchouk, M. E. Christy and C. E. Keppel, Phys. Rev. C **78** (2008) 025206.
- [26] S. P. Malace, Y. Kahn, W. Melnitchouk and C. E. Keppel, Phys. Rev. Lett. **104** (2010) 102001.
- [27] I. Niculescu *et al.*, arXiv:1501.02203 [hep-ex].
- [28] A. De Rujula, H. Georgi and H. D. Politzer, Annals Phys. **103** (1977) 315.
- [29] O. Nachtmann, Nucl. Phys. **B63** (1973) 237.
- [30] O. Nachtmann, Nucl. Phys. **B78** (1974) 455.
- [31] O. W. Greenberg and D. Bhaumik, Phys. Rev. D **4** (1971) 2048.
- [32] J. M. Cornwall and R. E. Norton, Phys. Rev. **177** (1969) 2584.
- [33] S. P. Malace *et al.*, Phys. Rev. C **80** (2009) 035207.
- [34] P. Monaghan *et al.*, Phys. Rev. Lett. **110** (2013) 152002.
- [35] M. E. Christy and P. E. Bosted, Phys. Rev. C **81** (2010) 055213.
- [36] S. Alekhin, J. Blümlein and S. Moch, Phys. Rev. D **86** (2012) 054009.

- [37] F. M. Steffens and W. Melnitchouk, Phys. Rev. C **73** (2006) 055202.
- [38] P. E. Bosted and M. E. Christy, Phys. Rev. C **77** (2008) 065206.
- [39] J. F. Owens, A. Accardi and W. Melnitchouk, Phys. Rev. D **87** (2013) 094012.
- [40] J. J. Kelly, Phys. Rev. C **70** (2004) 068202.
- [41] F. D. Aaron *et al.*, JHEP **1209** (2012) 061; H. Abramowicz *et al.*, Phys. Rev. D **87** (2013) 052014.
- [42] M. Virchaux and A. Milsztajn, Phys. Lett. B **274** (1992) 221.
- [43] S. I. Alekhin, S. A. Kulagin and S. Liuti, Phys. Rev. D **69** (2004) 114009.
- [44] P. Jimenez-Delgado and E. Reya, Phys. Rev. D **89** (2014) 074049.
- [45] N. L. Hall, P. G. Blunden, W. Melnitchouk, A. W. Thomas and R. D. Young, Phys. Lett. B **731** (2014) 287.
- [46] J. Alwall and G. Ingelman, Phys. Lett. B **596** (2004) 77.
- [47] J. J. Sakurai and D. Schildknecht, Phys. Lett. B **40** (1972) 121.
- [48] J. Mammei, Nuovo Cim. C035N04 (2012) 203.
- [49] F. Maas, talk presented at *PAVI 2014: From Parity Violation to Hadron Structure*, Skaneateles, New York, July 2014.